Contribution of Variable Speed Wind Turbine Generator Based on DFIG Using ADRC and RST Controllers to Frequency Regulation

Mohssine Chakib*‡, Tamou Nasser**, Ahmed Essadki*

** Electrical Engineering Department of High School of Technical Education (ENSET) Mohammed V University, Rabat, Morocco

** Communication Networks Department of National High School for Computer Science and Systems (ENSIAS) Mohammed V University, Rabat, Morocco

(chakib1mohssine@gmail.com, tamounasser@gmail.com, ahmed.essadki1@gmail.com)

‡ Corresponding Author, Mohssine Chakib, Morocco, Tel: +212 679 316 075,

chakib1mohssine@gmail.com

Received: 07.02.2021 Accepted:13.03.2021

Abstract- In the interconnected power systems, there must always be a balance between the amount of electricity produced and the amount of electricity consumed in order to keep the grid frequency stable and nearby to its nominal value. Therefore, any change in consumption can lead to imbalance, instability, load shedding and system frequency disturbances. With the increase of wind energy penetration level in the electrical network, it has become necessary to make wind generators participate in frequency regulation. The fundamental objective of this research paper is to investigate the ability of wind turbine at variable speed equipped with doubly fed induction generator (DFIG) to contribute in the grid frequency regulation. For the purpose of the contribution in the frequency regulation, the wind turbine system must inject a supplementary power support into the electrical network. To do that, two control strategies are adopted: the first one is the synthetic inertia control which uses the kinetic energy reserved and stocked in the turbine and generator rotors of the wind system. The second one is the droop frequency control which includes the deloading method that allows to the VSWT to create a certain reserve active power. Then, each of these control techniques is implemented and their performances are evaluated in case of frequency variation. Moreover, the control structure that uses the combination of these two techniques is also implemented and studied. The active disturbance rejection control strategy (ADRC), the classical PI controller and the polynomial RST controller have been adopted to command the rotor side converter (RSC) of the DFIG which allows it to provide, in case of frequency fault, a support for the power system into the grid by adjusting the rotor speed. The performance of these controllers are tested and compared and the simulation is performed by MATLAB/Simulink simulation software.

Keywords- Variable Speed Wind Turbine system, DFIG, Active Disturbance Rejection Control, inertia control strategy, droop control strategy, Deloading method.

1. Introduction

At present, the global wind power generation has experienced a substantial growth and has developed rapidly compared to other energy sources. Consequently, following the strong penetration of wind energy into the electrical system, the wind turbines generators must participate in frequency stabilization in the event of an imbalance between the electrical energy produced and that consumed [1].

Currently, the most famous wind generators used are the variable speed wind generators equipped with the DFIG due to their maximum power tracking operation and their ability to regulate easily and independently the active power and reactive power injected to the electrical network by using converters [2].

The DFIG is subject to the effects of generator parametric uncertainty (that can be caused by saturation effect, skin effect, overheating effect, etc.), and the effect of disturbance due to the speed variation [3]. To overcome these constraints, the used controller should be robust and efficient.

With the increased penetration of wind turbines into the electrical power grid, the wind generators replace a large number of conventional generation units such as synchronous generators. In addition, these types of wind generators are insensitive to frequency variations owing to the decoupling of DFIG rotor speed and the electrical grid frequency [4]. Therefore, the total inertia of the system is decreased and the ability to maintain power system frequency stability is degraded when a frequency disturbance occurs. Several researches have addressed this issue by proposing several control schemes that allow wind turbines systems to involving into primary frequency control [4-5]. Two categories of these schemes are notably essential for involving variable speed wind generators in the frequency setting, they are classified into: Synthetic inertial control and primary droop controller [5].

The inertial control which essentially uses the kinetic energy stockpiled in the wind turbine blades and the rotor of DFIG allow adding an additional active power so as to correct the frequency drop during the initial time [5-6].

Besides, the primary droop control which liberates the reserved power in wind turbine generator in order to compensate the system frequency deviation by providing automatically an active power support [6]. Therefore, the WTG must be operating at de-loaded conditions through setting the parameters of the maximum power point tracking (MPPT) so that we can obtain an active power reserve [7].

Several studies have shown that the ADRC control strategy is characterized by very good robustness and that it has a good efficiency in set points tracking because it has many advantages, such as good performance and high accuracy in case of dynamic system control, system stability ensured and the easy implementation thanks to the tuning parameters reduced [8]. The ADRC method typically uses an Extended Status Observer (ESO) which acts as a status feedback controller and provides the system status information in real time and it allows estimating and deleting all internal and external disturbance can affect the system [8-9].

In this work, the first-order ADRC control strategy has been used so as to command the rotor side converter (RSC) of DFIG. Furthermore, in order to make wind turbine participate in frequency control, inertia and primary droop control strategies are implemented in the RSC of the DFIG based wind turbines in order to adjusting the rotor speed when a frequency disturbance occurs "Fig. 1".

This article is structured into five sections as follows: We start, in the second Section, with modeling of different components of DFIG based variable speed wind turbine. Moreover, the structures of the RST and ADRC control methods are described and these control strategies are applied to the RSC so as to control the active and reactive power of DFIG. In Section 3, the operation at de-loaded mode of wind turbine, the strategies of frequency control (inertia and droop control) and combination of them are presented. Then the section 4 presents and compares the results and tests of simulation which were carried out using MATLAB/Simulink environment. Finally, Section 5 concludes and summarizes this research.

2. Modeling and control of DFIG wind turbine

2.1. Wind turbine modeling

The aerodynamic model of the wind turbine is modeled mathematically by the following equation [9, 24]:

$$P_t = \frac{1}{2} C_p(\lambda, \beta) A \rho V^3 \quad (1)$$

Where, A is the rotor blades swept area in m^2, V is wind speed in m/s, ρ is air density in kg/m3 and C_p is power coefficient is given as follows "Eq.2" [9]:

$$C_p = 0.5176\left(\frac{116}{\lambda_i} - 0.4\beta - 5\right) e^{\left(-\frac{21}{\lambda_i}\right)} + 68.10^{-4}\lambda \quad (2)$$

Where:

β: The pitch angle.

λ_i is given as follows "Eq.3":

$$\frac{1}{\lambda_i} = \frac{1}{\lambda + 0.08\beta} - \frac{0.035}{1+\beta^3} \quad (3)$$

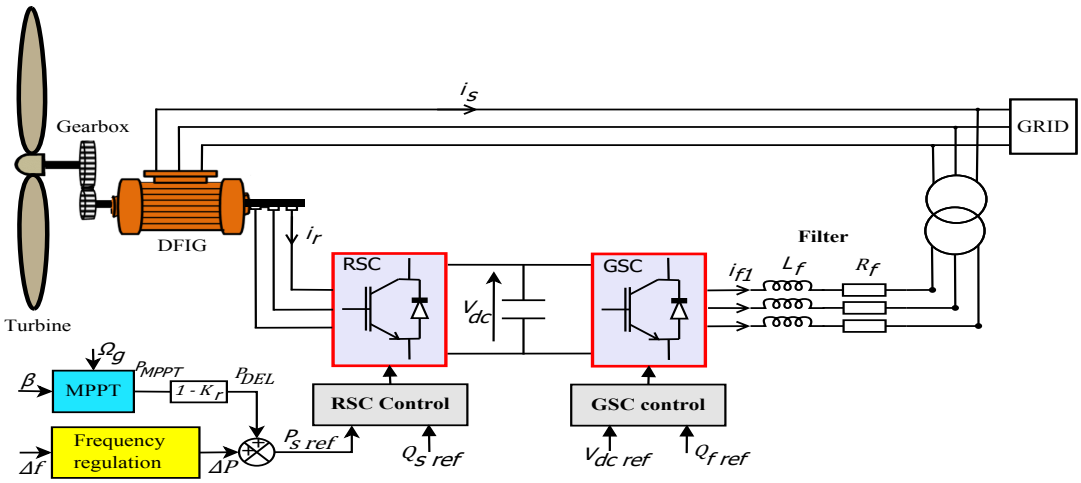

Fig. 1. Control scheme of DFIG based variable speed WT with frequency regulation.

And λ is the tip speed ratio [24]; it is given by "Eq.4":

$$\lambda = R\frac{\Omega_t}{V} \tag{4}$$

Where:

Ω_t: Turbine rotor speed.

R: Rotor radius

The fundamental principle of the dynamics is defined as follows [10-11]:

$$J\frac{d\Omega_g}{dt} = T_g - T_{em} - f_v\Omega_g \tag{5}$$

Where:

T_{em}: The electromagnetic of generator,

T_g: The mechanical torque of DFIG rotor,

Ω_g: The mechanical speed of DFIG rotor,

f_v: The viscous friction coefficient,

J: The total inertia.

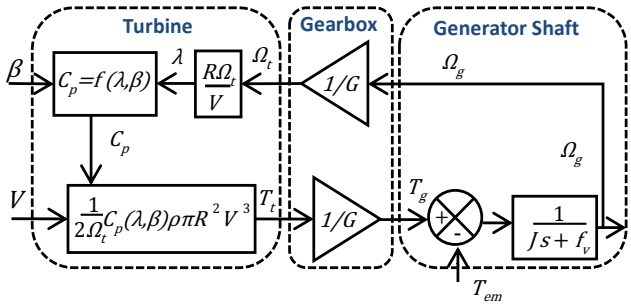

Fig. 2. Wind turbine converter model.

2.2. DFIG modelling

The DFIG is used to convert the mechanical rotation of the wind turbine (WT) into electric power.

By considering the following assumptions [9]:

- The stator resistance R_s is neglected,
- The stator flux vector ϕ_s is oriented along the d axis.

This generator is modeled in d-q reference frame by "Eq.6" to "Eq.9" [9-10, 25, 27].

$$\begin{cases} \phi_{sd} = L_s I_{sd} + L_m I_{rd} = \phi_s \\ \phi_{sq} = L_s I_{sq} + L_m I_{rq} = 0 \\ \phi_{rd} = L_r I_{rd} + L_m I_{sd} \\ \phi_{rq} = L_r I_{rq} + L_m I_{sq} \end{cases} \tag{6}$$

$$\begin{cases} V_{sd} = R_s I_{sd} + \frac{d\phi_{sd}}{dt} - \omega_s \phi_{sq} = 0 \\ V_{sq} = R_s I_{sq} + \frac{d\phi_{sq}}{dt} + \omega_s \phi_{sd} = \phi_s \omega_s \\ V_{rd} = R_r I_{rd} + L_r \sigma \frac{dI_{dr}}{dt} - g\omega_s L_r \sigma I_{rq} \\ V_{rq} = R_r I_{rq} + L_r \sigma \frac{dI_{rq}}{dt} - g\omega_s L_r \sigma I_{rd} + g\frac{V_s M}{L_s} \end{cases} \tag{7}$$

Where:

$$\sigma = 1 - \frac{M^2}{L_s L_r} \tag{8}$$

And:

$$\begin{cases} P_s = -V_s \frac{M}{L_s} I_{rq} \\ Q_s = -V_s \frac{M}{L_s} I_{rd} + \frac{V_s^2}{L_s \omega_s} \\ T_{em} = -p\frac{M}{L_s}\phi_s I_{rq} \end{cases} \tag{9}$$

Where:

P_s, Q_s: Active and reactive power of stator,

V_r, V_s: Stator and rotor voltages,

ϕ_s, ϕ_r: Stator and rotor fluxes,

I_s, I_r: Stator and rotor currents,

ω_s, ω_r: Stator and rotor angular frequency,

R_r: Rotor resistance,

L_s, L_r: Stator and rotor inductances,

M: Mutual inductance,

p: Pole pairs number

2.3. Active disturbance rejection controller (ADRC)

The ADRC strategy is a robust controller that includes an extended state observer (ESO) allows estimating and rejecting any unexpected disturbance "Fig.3" [8-9].

The expression of the linear first-order ADRC control is obtained as "Eq.10" [9]:

$$\dot{y} = f(y, d, t) + bu \tag{10}$$

Where u is control input, y is the system output, d is the external disturbance, f is the total disturbance and b is the control gain [8-9].

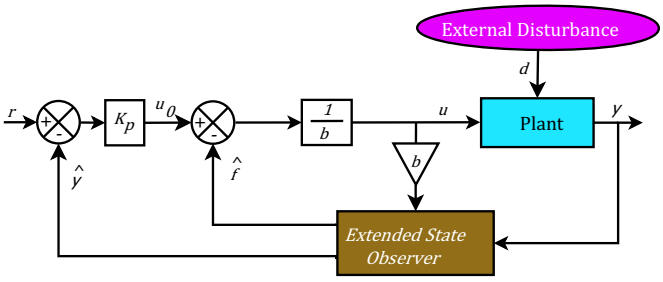

Fig. 3 ADRC controller structure

The linear first order extended state observer (ESO), expressed by "Eq.11", allows obtaining the estimates of f and y [9].

$$\begin{cases} \dot{\hat{y}} = \hat{f} + \beta_1(y - \hat{y}) + b_0 u \\ \dot{\hat{f}} = \beta_2(y - \hat{y}) \end{cases} \tag{11}$$

Where, β_1 and β_2 are the gains of the observer "Eq.12":

$$\begin{bmatrix} \beta_1 \\ \beta_2 \end{bmatrix} = \begin{bmatrix} -2\omega_0 \\ \omega_0^2 \end{bmatrix} \tag{12}$$

ω_0 is the bandwidth of the ESO.

$$\omega_0 = 3 \sim 7\, K_p \tag{13}$$

Where, K_P is the ADRC control parameter.

The rotor currents of DFIG can be written in the following form [9]:

$$\begin{cases} \dot{I}_{rd} = \frac{1}{\sigma L_r} V_{rd} - \frac{R_r}{\sigma L_r} I_{rd} + \omega_r I_{rq} = f_1(t) + bu_1 \\ \dot{I}_{rq} = \frac{1}{\sigma L_r} V_{rq} - \frac{R_r}{\sigma L_r} I_{rq} - \omega_r I_{rd} - \frac{M\omega_r}{\sigma L_r L_s} \phi_{sq} = f_2(t) + bu_2 \end{cases} \quad (14)$$

Where:

$$\begin{cases} f_1(t) = -\frac{R_r}{\sigma L_r} I_{rd} + \omega_r I_{rq} \\ f_2(t) = -\frac{R_r}{\sigma L_r} I_{rq} - \omega_r I_{rd} - \omega_r \frac{M}{\sigma L_r L_s} \phi_{sq} \\ u_1 = V_{rd} \quad ; u_2 = V_{rq} \quad ; \quad b = \frac{1}{\sigma L_r} \end{cases} \quad (15)$$

The "Fig. 4" depicts the indirect control of the stator powers of DFIG through control of the DFIG rotor currents using ADRC controller [9].

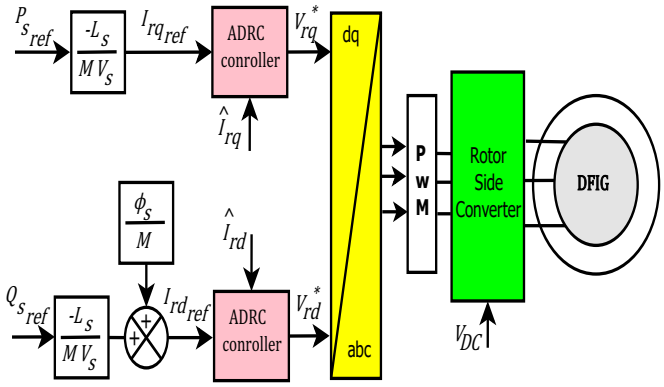

Fig. 4. Scheme of DFIG power control using linear ADRC.

The RSC is controlled by the Sinusoidal Pulse Width Modulation technique.

2.4. RST polynomial control

The RST polynomial control is a linear controller composed of three polynomials R, S and T whose coefficients are determined so that we can get an effective control. The general RST controller structure is shown in "Fig.5" [9].

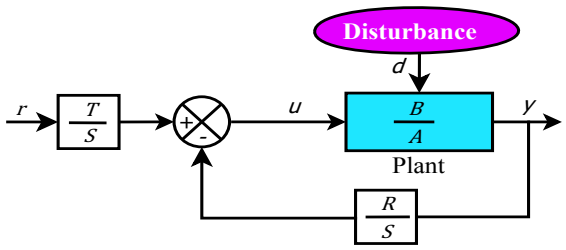

Fig. 5. RST controller structure.

Where *r* is the reference input and *y* is the system output.

The transfer function of the DFIG system is given by "Eq.16":

$$\frac{B(s)}{A(s)} = \frac{MV_s}{L_s R_r + sL_s L_r \sigma} \quad (16)$$

The expressions of the control polynomials are given as follows [9]:

$$\begin{cases} R(s) = r_1 s + r_0 \\ S(s) = s_2 s^2 + s_1 s + s_0 \\ T(s) = T_0 \end{cases} \quad (17)$$

The coefficients of these polynomials are determined by solving the following equation called Bezout equation "Eq.18" [9].

$$\begin{cases} D(s) = A(s).S(s) + B(s).R(s) = C(s).F(s) \\ D(s) = (s - s_c)(s - s_f)^2 \end{cases} \quad (18)$$

Where, *C(s)* and *F(s)* are respectively the control polynomial and the filtering polynomial.

Generally:

$$s_c = 5\, s_A \quad ; \quad s_f = 3\, s_c = 15\, s_A \quad (19)$$

From the "Eq.16" to "Eq.19", we obtain the parameters of RST control [9]:

$$\begin{cases} s_2 = \frac{1}{L_s L_r \sigma} \\ s_1 = \frac{35 R_r}{L_s (L_r \sigma)^2} \\ s_0 = 0 \\ r_1 = \frac{340 {R_r}^2}{MV_s (L_r \sigma)^2} \\ r_0 = T_0 = \frac{1125 {R_r}^3}{MV_s (L_r \sigma)^3} \end{cases} \quad (20)$$

The "Fig. 6" depicts the direct control of the stator powers produced by the DFIG using RST control [9].

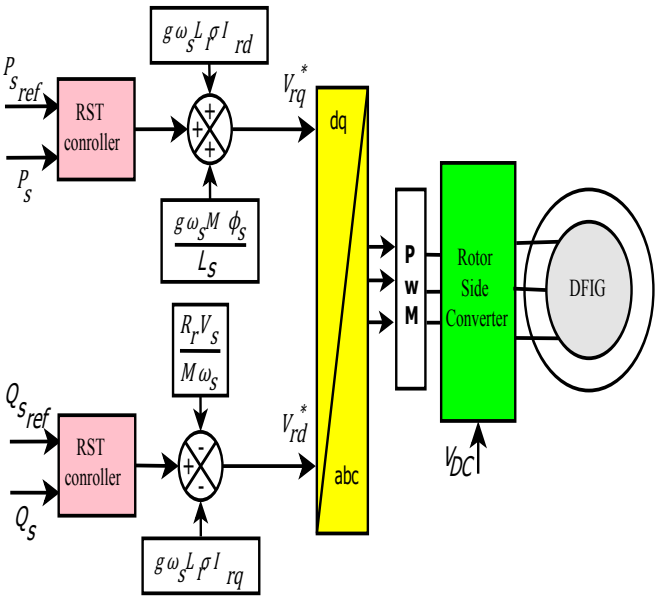

Fig. 6. Scheme of DFIG power control using RST control.

3. Primary frequency regulation strategies

3.1. Inertial control strategy

This control strategy permits the turbine-generator to release the energy stored in the WT rotating masses to the power system at the event of frequency disturbance "Fig. 7" [6,11]. Its principle consists in obtaining a new reference of electromagnetic torque, so a new active power reference, from the rate of variation of frequency. In case of a frequency drop, the reference electromagnetic torque rises, bringing about a deceleration of the DFIG rotor speed. Therefore, supplying a portion of the kinetic energy stored in the rotating objects of WT [11].

Its principle consists in obtaining of the electromagnetic torque, so of active power, from the rate of variation of frequency. In case of a frequency drop, the reference electromagnetic torque increases.

The new set point power is expressed as follows:

$$P_{s_{ref}} = P_{MPPT} + \Delta P_{IN} \tag{21}$$

Where ΔP_{IN} is the support inertial, it is expressed as [11-12,18]:

$$\Delta P_{IN} = -2K_{IN}\, f_{meas} \frac{df_{meas}}{dt} \tag{22}$$

We have added a block called dead zone which generates zero output when the frequency deviation is less than 0.075 Hz [17], in order to activate the frequency controller only if the frequency deviation exceeds this limit.

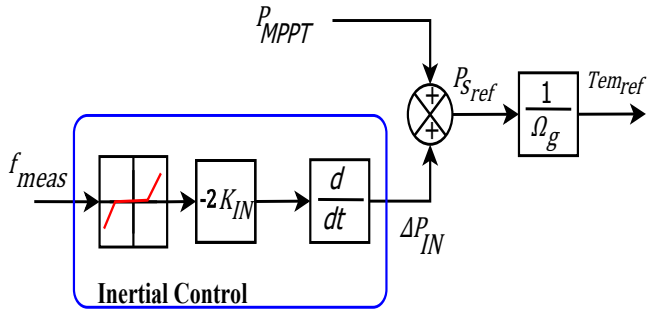

Fig. 7. Block diagram of inertial control strategy.

3.2. De-loading operation of Variable Speed WTGs

Thanks to this control strategy, an active power reserve is obtained by moving the WT from the maximum operating point PMPPT to another operating point in deloloading mode PDEL "Fig. 8" [12-13]. This active power reserve ΔP_{RES} will be used to help restore the system frequency after a disturbance [13]. This method uses a new reference of the electromagnetic torque unlike MPPT operation.

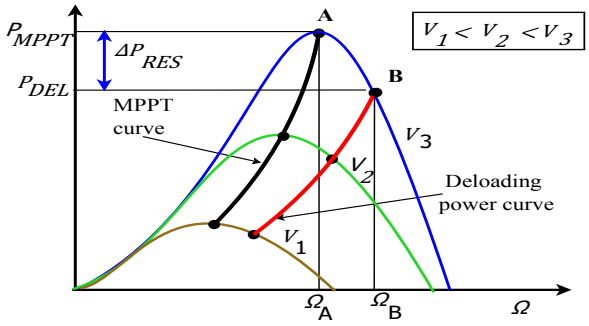

Fig. 8. MPPT and deloading power curve of variable speed WT.

The deloaded power is expressed by the following equation:

$$P_{DEL} = (1 - K_r) P_{MPPT} \tag{23}$$

Where:

$$P_{MPPT} = \frac{1}{2} C_{p_{max}}(\lambda_{opt}, 0)\rho\pi R^2 V^3 \tag{24}$$

Thus, the power coefficient reference in deloaded mode is given by "Eq.25":

$$C_{p_{del}}(\lambda_{del}, 0) = (1 - K_r) C_{p_{max}}(\lambda_{opt}, 0) \tag{25}$$

Where, Kr is the reserve factor.

In this study, we chose: K_r=15%

Thus, the electromagnetic torque reference can be expressed by "Eq.26":

$$T_{em_{del}} = \frac{P_{s_{ref}}}{\Omega_g} = \frac{1}{2\Omega_g} C_{p_{del}}(\lambda_{del}, 0)\rho\pi R^2 \left(\frac{R\,\Omega_g}{G\lambda_{del}}\right)^3 \tag{26}$$

3.3. Droop control strategy

Droop control principle consists in providing a supplementary active power proportional to frequency variations "Fig. 9". It is expressed as follows [14, 16]:

$$\Delta P_{droop} = K_d\, \Delta f = K_d\, (f_{ref} - f_{meas}) \tag{27}$$

Where K_d is the droop gain, it is given as follows [15-16, 26].

$$K_d = \frac{P_n}{\delta . f_{ref}} \tag{28}$$

Where δ is the droop parameter

We chose δ=4%

Taking into account the primary frequency adjustment, the new electromagnetic torque reference become as follow:

$$T_{em_{ref}} = \frac{1}{2\Omega_g} C_p(\lambda, 0)\rho\pi R^2 \left(\frac{R\,\Omega_g}{G\lambda}\right)^3 \tag{29}$$

Where:

$$C_p(\lambda, 0) = C_{p_{del}}(\lambda_{del}, 0) + \Delta C_p \tag{30}$$

$$C_p(\lambda, 0) = (1 - K_r) C_{p_{max}} + \frac{\Delta P_{droop}}{0.5\rho\pi R^2 V^3} \tag{31}$$

And the ratio speed λ is obtained by solving the expression of the power coefficient C_p at β=0°, obtained by interpolation polynomial method [22]:

$$C_p(\lambda) = a_1\lambda^2 + a_2\lambda + a_3 \quad (32)$$

Where:

$$\begin{cases} a_1 = -0.0158 \\ a_2 = 0.2508 \\ a_3 = -0.5302 \end{cases} \quad (33)$$

$$\lambda = max\left(\frac{-a_2 \pm \sqrt{a_2^2 - 4a_1(a_3 - C_p)}}{2a_1}\right) \quad (34)$$

The droop frequency control can solely be activated when the deviation of frequency is outside a specific bound (in our case: $|\Delta f| > 0.075$Hz) [17].

The new power reference of DFIG "Fig. 10" is given by the following equation:

$$P_{s_{ref}} = T_{em_{ref}}.\Omega_g = P_{DEl} + \Delta P_{droop} \quad (35)$$

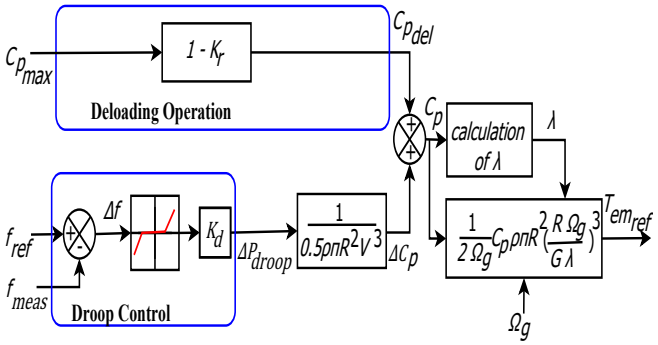

Fig. 9. Block diagram of droop control strategy

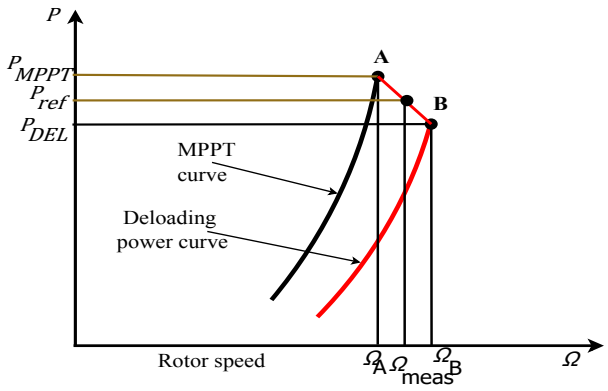

Fig. 10. Power reference of WTG using Droop control

3.4. Combined inertia-droop control strategy

The combined control scheme consists in combining the inertia control and the droop control in order to obtain a single electromagnetic torque reference and hence only an active power reference [19]. Therefore, we will benefit of both inertial support and primary power reserve support"Fig.11".

The electromagnetic torque setpoint can be defined by "Eq. (36)":

$$T_{em_{ref}} = \frac{P_{s_{ref}}}{\Omega_g} = \Delta T_{em_{in}} + T_{em_{dr}} \quad (36)$$

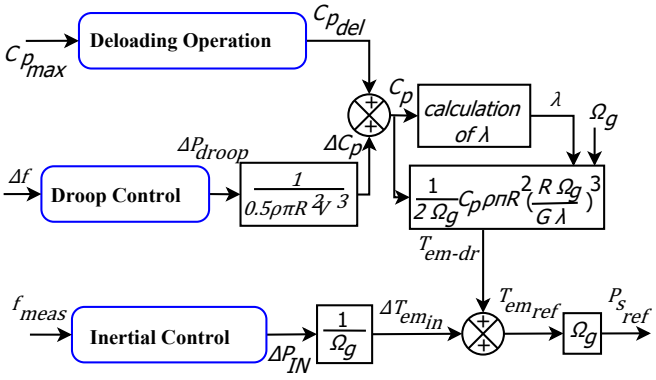

Fig. 11. Block diagram of combined inertial and droop controller.

4. Simulation results, analysis and discussion

4.1. Modeling of studied power system

In order to investigate the performance of the used control techniques, we consider a small electrical power system composed of a thermal generator based on the reheat steam turbine and the wind generation system based on the DFIG generator, the diagram of the adopted system frequency response is depicted in the following figure [20-21]. The simulations were performed using Matlab/Simulink software.

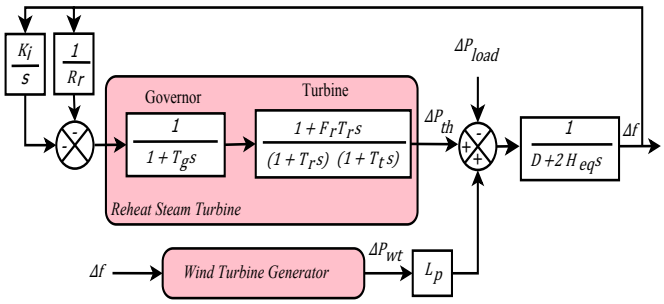

Fig. 12. Studied system frequency response model.

Note that this system operates without automatic generation control (AGC) therefore its coefficient Ki is assumed to be zero in the studied system, because we are only interested in the primary frequency regulation in this study.

All the simulation parameters are listed in "Table 2." to "Table 4."

4.2. Overview and description of frequency response metrics

The important metrics "Fig.13" of the frequency response, when there is a sudden diminution in power generation, are as follows:

- **Rate of change of frequency (RoCoF):** This is the frequency decline rate $\frac{df}{dt}$.
- **Frequency nadir:** This is the lowest frequency in the response.
- **Settling frequency:** This is the average frequency after the event.

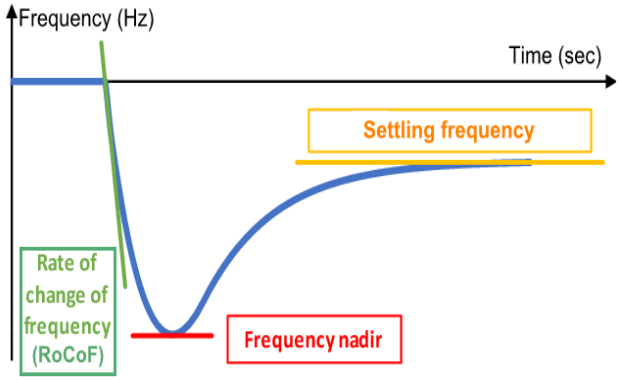

Fig. 13. Metrics of frequency response curve

4.3. Effect of the wind turbine penetration level on the electric grid

In order to show the need for a frequency control of the variable speed wind turbine generator (VSWTG), for support and regulate the system frequency in the event of a fault, we tested the effect of rising in the penetration level (L_p) of VSWTG in the grid on the frequency response during an unexpected frequency drop. We are considered that only the thermal generator that participates in system frequency regulation and the system has undergone a sudden load increase of 0.1 pu is introduced at t = 15 sec.

The "Fig.14" shows that the high wind penetration level causes the increase in the frequency deviation. Also the frequency nadir of the network reaches a deeper value (f_{NADIR} =49.17 Hz) in the case of L_p =30%. This problem is caused by electronics converters that decouple the VSWT from the power system which leads to decreasing the global grid inertia because the power system is deprived from the inertia support that could be given by the VSWTG. Hence the need to apply a frequency control loop.

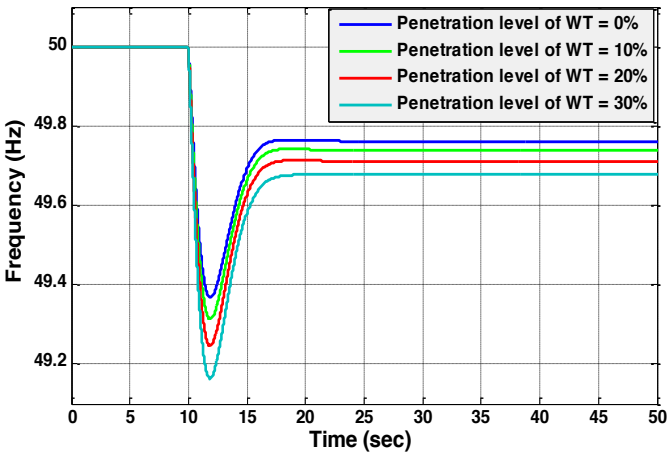

Fig. 14. System frequency for various values of L_p without contribution of VSWT in frequency regulation.

4.4. Effect of the frequency regulation techniques of WTG on frequency response

The frequency response of the power system consisting of a WTG and a thermal generator "Fig .12" is studied so as to evaluate and compare the frequency control strategies of WTG. Four simulation scenarios are carried out:

- **Scenario 1**: Wind turbine generator (WTG) without any frequency control strategy and only the thermal generator can participate in the frequency support.
- **Scenario 2**: Inertial-support control method of the WTG was enabled.
- **Scenario 3:** Speed droop control method of the WTG was enabled.
- **Scenario 4**: The both controllers (inertia and droop control) were simultaneously enabled.

These different scenarios have been simulated for various wind power penetration levels (L_p=10%, 20%, 30% and 45%) as depicted in "Fig .15" to "Fig .18".

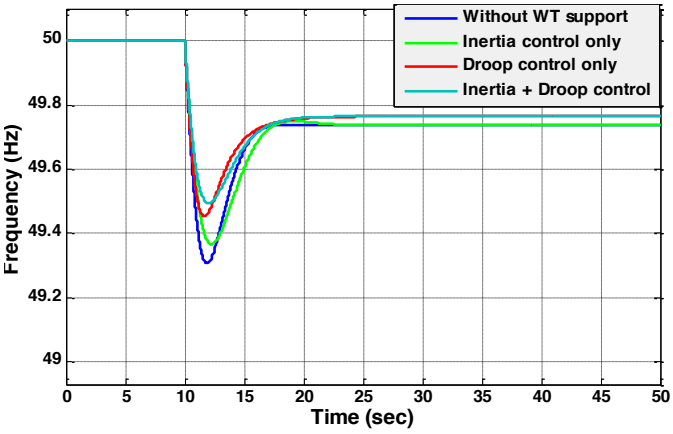

Fig. 15. Frequency response for L_p=10%

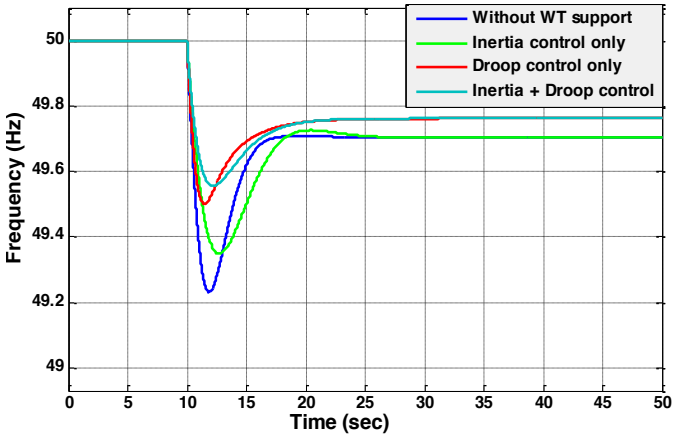

Fig. 16. Frequency response for L_p =20%

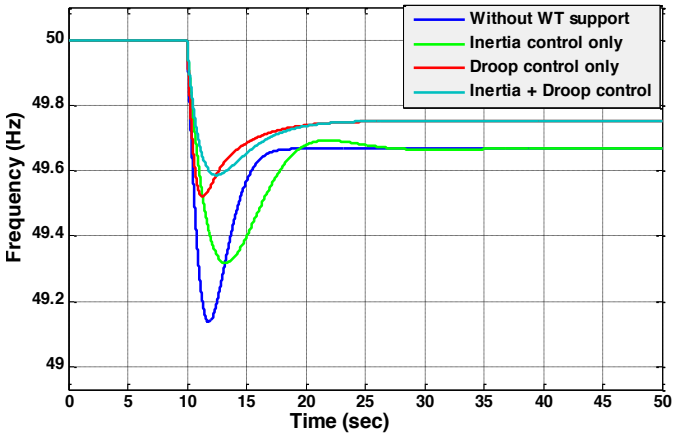

Fig. 17. Frequency response for L_p =30%

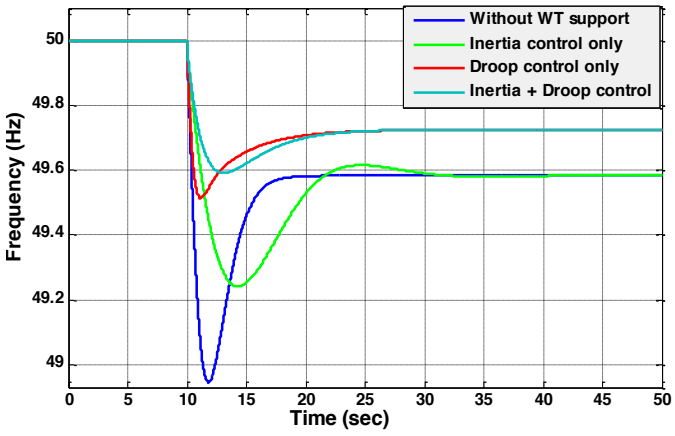

Fig. 18. Frequency response for L_p =45%

To analyze these results, we must compare the performance metrics of these frequency responses. To do this, we start by calculating the RoCoF as shown in "Fig .19" to "Fig .22". Then we plot the variation of the performance metrics for each case.

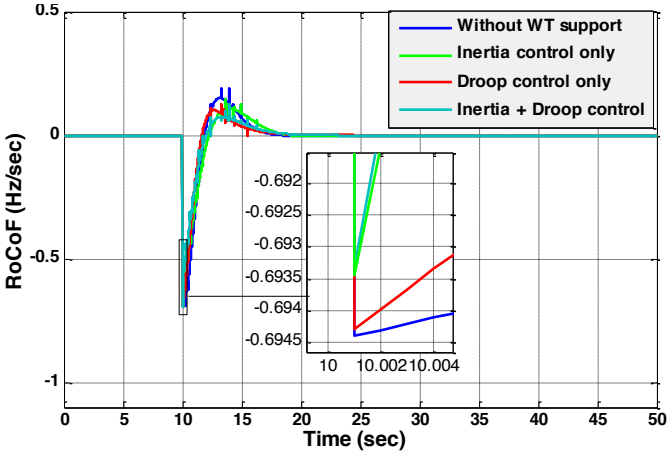

Fig. 19. RoCoF for L_p =10%

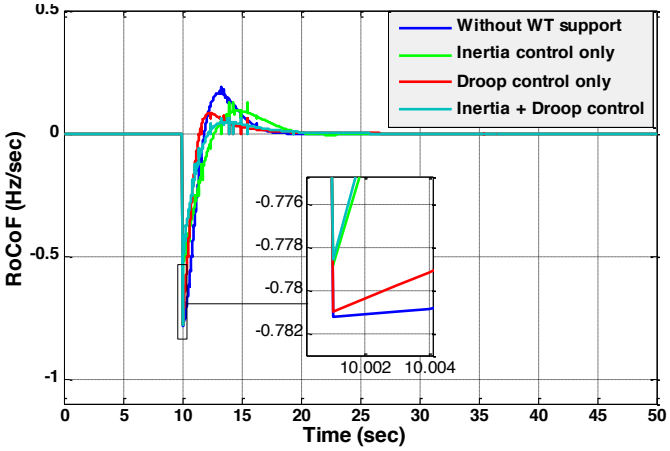

Fig. 20. RoCoF for L_p =20%

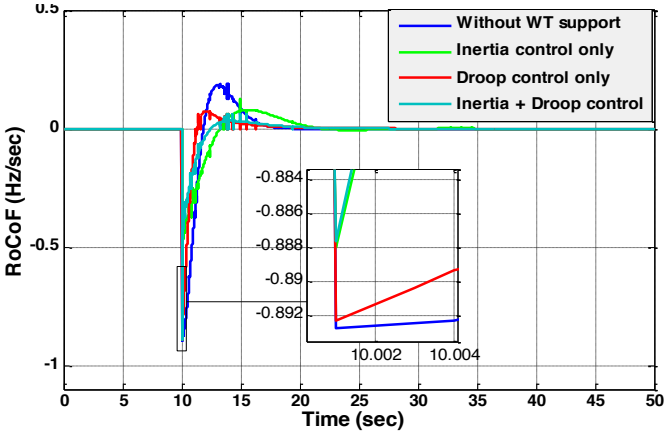

Fig. 21. RoCoF for L_p =30%

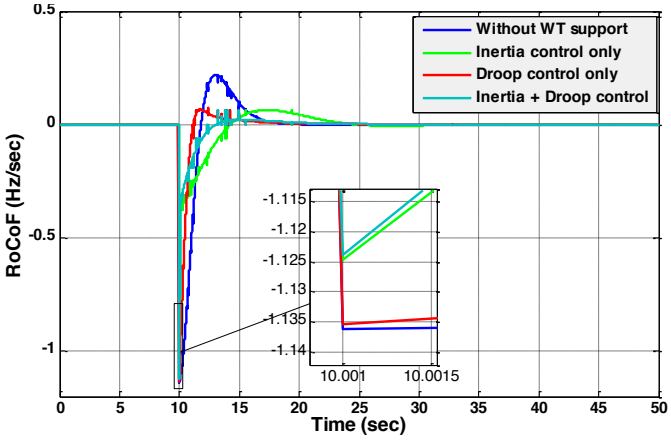

Fig. 22. RoCoF for Lp=45%

The "Fig.23" summarizes the metrics of the frequency response (nadir, RoCoF and settling frequency) as a function of WT penetration levels (L_p) for the various simulation cases.

In the **first scenario** (without any WTG support), the "Fig. 23a" and "Fig. 23b" show that the frequency nadir and also the settling frequency decrease with increasing penetration level of wind generation because the WT power is not sensitive to the frequency variation. On the other hand, the ROCOF increases "Fig. 23c" when the penetration level of WTG increases.

In the **second scenario** (inertial support WTG), the inertial frequency control brought a significant improvement of the frequency nadir especially in higher wind penetration as shown in "Fig. 23a". On the other hand, in steady state, we note that there is no difference in the settling frequency compared of the first scenario due to the rapid exhaustion of the stored kinetic energy in the rotating masses of WTG "Fig. 23b". Therefore, the inertia support contributes to reduce the declining of RoCoF when the disturbance occurs as shown in "Fig. 23c".

Figure 24 and Figure 25 show that when the frequency decreases, the mechanical speed decelerates as to allow the WT to increase production by excerpting a portion of the kinetic energy reserved in the rotating masses. This supplementary power support will aid the system for a short time (17s). In steady state, the frequency stabilizes and the active power returns to its initial setpoint.

In the **third scenario** (Droop control only), the wind turbine operates under the optimal operating point so as to create the power reserve "Fig.24". This power reserve is injected into the grid immediately when the disturbance occurs "Fig.24", which brings about a diminution in rotor speed "Fig.25". The "Fig. 23a" and "Fig. 23b" show that the both parameters of frequency: setting value and the nadir frequency are increased with increasing of wind penetration level. So there is an improvement of the frequency response in the steady state. Furthermore, Figure "Fig. 23c" shows that this control method contributes to a little decrease in the decline of RoCoF compared to inertial control.

In the **fourth scenario** (Combination of inertia and droop controls), the suggested combination of the both controllers offers a good and more improvements than the results of the previous scenarios for the three main frequency metrics, such as: a greater reduction in the drop in RoCoF, the best nadir and settling frequency "Fig. 23".

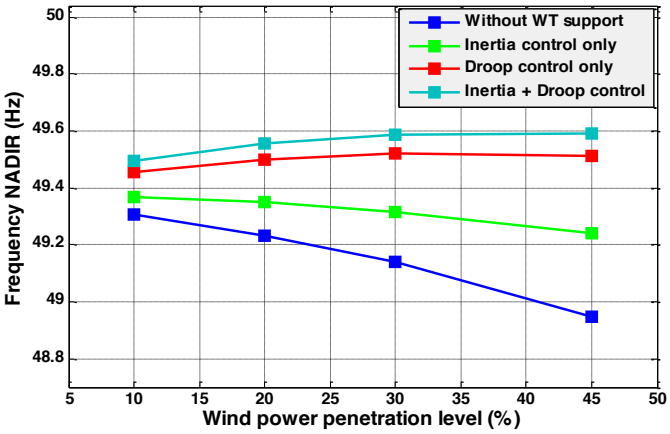

(a)

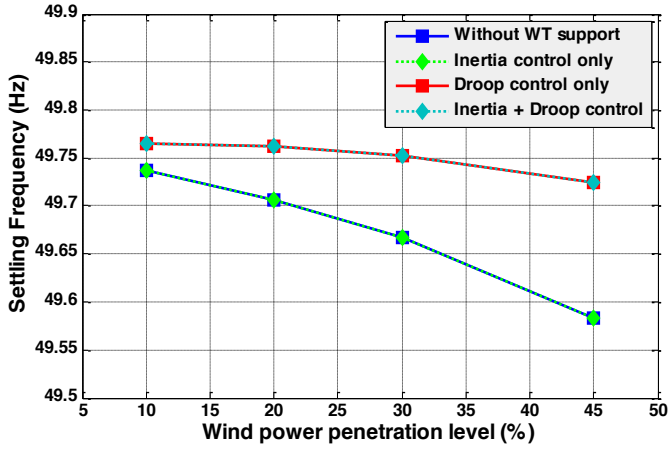

(b)

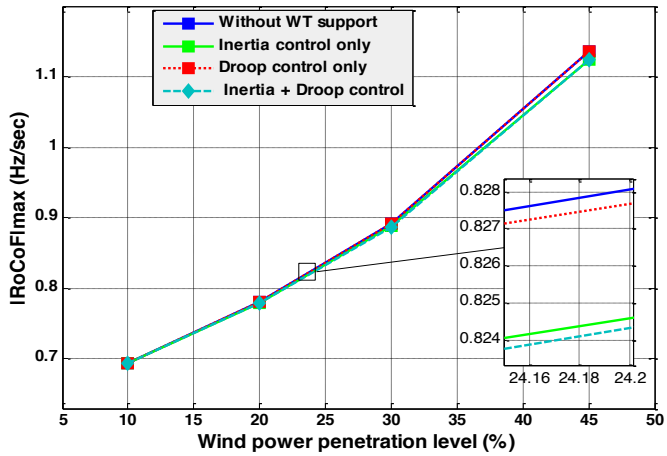

(c)

Fig. 23. Impact of wind active power controls, for different penetration levels, on: (a) frequency nadir, (b) settling frequency and (c) maximum ROCOF.

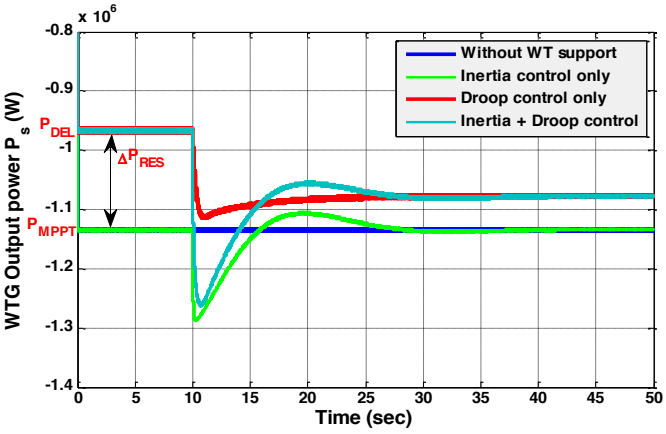

Fig. 24. WT active power evolution for different frequency control strategies

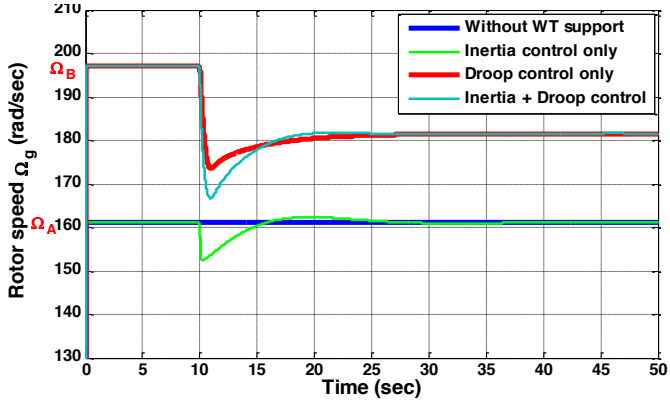

Fig. 25. Rotor speed evolution for different frequency control strategies

4.5. Performance evaluation of the proposal controllers RST and ADRC used to control the WT based on DFIG

The simulation results of the active and reactive powers of DFIG stator are respectively illustrated in "Fig. 26" to "Fig. 27". We can see that the responses obtained by the ADRC controller follow with high performance their references with zero overshoot, a time stabilization, recovery time and rise time, shorter than RST and PI controllers. In addition, the performance of RST control is better than the classic PI control. In terms of robustness, the obtained results prove that the ADRC controller is more robust and it adapts very well to load disturbances and speed variations compared to the other controllers tested. So the ADRC controller has a great disturbance rejection capability and high performance in term of reference tracking.

The "Table 1" gives a numerical comparison of the performance of PI, RST and ADRC controllers for the active power response of the DFIG stator.

Table 1. Active power response parameters.

Type of Controller	PI	RST	ADRC
Rise Time (s)	0.085	0.05	0.026
Settling time (s)	0.22	0.052	0.026
Overshoot (%)	12.3	0	0
Steady state error (%)	2.33	0.08	0.01

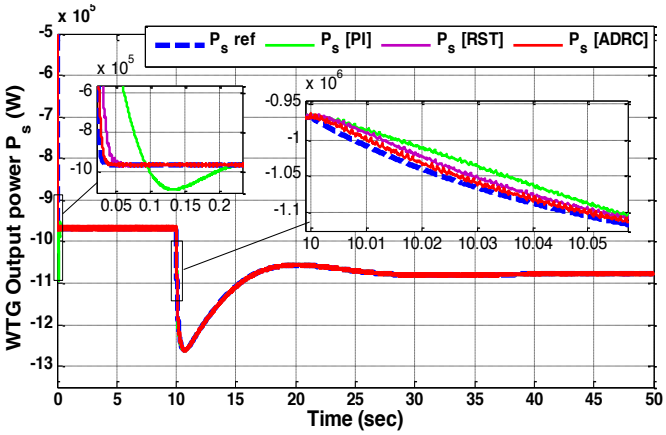

Fig. 26. WT active output power

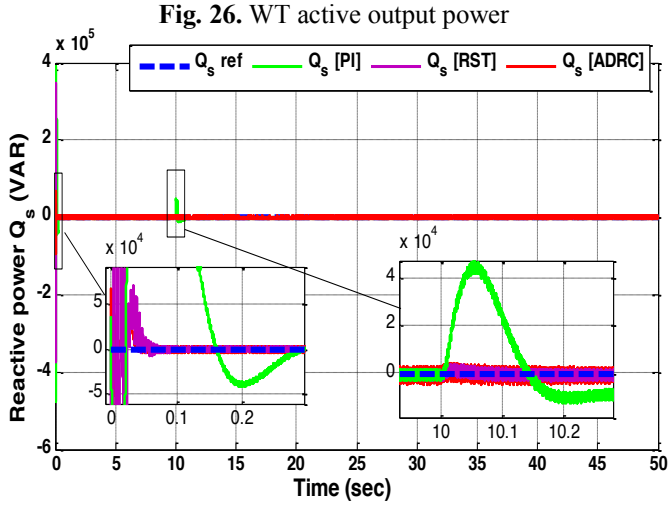

Fig. 27. WT reactive output power.

5. Discussions

The simulations results show that the inertia frequency control provides only a short-term frequency support which allows an important improvement in the frequency nadir, especially with a higher level of wind penetration. Although, with the speed droop control which uses the primary power reserve, it can be observed that the participation of the WT is higher, it also contributes to the stabilization of the frequency for a longer time but not only during the dynamics transients.

The suggested combination of the two controllers provides a good improvement for the three main frequency metrics, such as: important reduction of RoCoF dip, shallow nadir, and better stabilization frequency.

Regarding the DFIG control techniques, we can deduce that the proposed ADRC method gives better performance and it offers a good transient state in comparison with the PI and RST control methods.

6. Conclusion

In this work, a modeling of the WT system based on DFIG is presented. Also, this work explored and compared different active power control strategies that allow DFIG-based WT generator to participate in frequency regulation via the rotor speed adjusting. In a short period of time, the inertia

control strategy allows the wind turbine to emulate the behavior of synchronous generator. As a result, in the case of a frequency deviation, the controller commands the deceleration of the wind generator to pull out some of its kinetic energy, furnishing an additional active power support for power system. The droop control permits the WTG to furnish a power support over a prolonged period of time that allows enhancing the system robustness. In this case, the wind generator must function in deloaded mode in order to create some power reserve which may be provided automatically in the case of frequency excursions. The combined control (droop and inertial controls) enhances the frequency response demeanor. In this respect, the deloading mode of WT conduces to the rise in the rotor speed. Therefore, the inertial response was significantly enhanced thanks to the increase in the kinetic energy accumulated in the rotating objects.

Furthermore, in order to confirm and evaluate the efficiency of the ADRC control, comparisons with the PI and RST controllers are introduced in term of tracking the set point powers given by the frequency regulation strategies. The simulation results show that the proposed ADRC controller gives a very smaller steady state error, a faster response with very small overshoot compared to PI and RST controllers. Also, this controller has a good robustness against the disturbances.

Appendix

Table 2. DFIG and turbine Parameters [10]

Parameters	Values
Rated power	P_n= 1.5 MW
Number of pole pairs	p= 2
Rated stator voltage	398/690 V
Stator resistance	R_s = 0.012 Ω
Rotor resistance	R_r = 0.021 Ω
Stator inductance	L_s = 0.0137 H
Rotor inductance	L_r = 0.01367 H
Mutual inductance	M = 0.0135 H
Nominal frequency	f = 50 Hz
DC link voltage	V_{dc} = 1200V
Density of ajir	ρ = 1.225 kg/m^3
Damping coefficient	f_v = 0.0024
Gearbox ratio	G = 90
Turbine diameter	D = 70.5 m
Moment of inertia	J = 10 kg.m^2

Table 3. ADRC Control Parameters

Parameters	Values
Gain of controller K_p= S_{CL}	K_p= S_{CL} = 400
Poles of ESO	S_{ESO}= 5S_{CL} = 2000
Gains of the Extended State Observer (ESO)	β_1=2 S_{ESO} = 4000
	β_2= S_{ESO}^2= 4000000

Table 4. Parameters of the thermal generator

Parameters	Values
Governor time constant	T_g= 0.2 s
Reheat time constant	T_r= 7 s
Steam chest time constant	T_t= 0.3 s
High-pressure turbine fraction	F_r= 0.3
Inertia	H= 4 s
Load damping coefficient	D = 1
Governor speed regulation	R = 0.05
Integral gain	K_i= 0

References

[1] A. Molina-Garcia, I. Muñoz-Benavente, A. D. Hansen, E. Gómez-Lazaro, "Demand-Side Contribution to Primary Frequency Control with Wind Farm Auxiliary Control", *IEEE Transactions on Power Systems*, Vol.29, No.5, pp.2391-2399, 2014.

[2] M. Shahabi, M. R. Haghifam, M. Mohamadian, S. A. Nabavi-Niaki, "Microgrid Dynamic Performance Improvement Using a Doubly Fed Induction Wind Generator", *IEEE Trans. Energy Convers.*, Vol.24, No.1, pp.137-145, 2009.

[3] Y. Wang, Q. Wu, W. Gong, M. P. S. Gryning, "H∞ Robust Current Control for DFIG-Based Wind Turbine Subject to Grid Voltage Distortions", *IEEE Trans. on Sustainable Energy*, Vol.8, No.2, pp. 816 - 825, 2017.

[4] Y. Fu, X. Zhang, Y. Hei, H. Wang, "Active participation of variable speed wind turbine in inertial and primary frequency regulations", *Electric Power Systems Research*, Vol.147, pp.174-184, 2017.

[5] J. Morren, S.W.H. de Haan, W.L. Kling, J.A. Ferreira, "Wind Turbines Emulating Inertia and Supporting Primary Frequency Control", *IEEE Trans. Power Systems*, Vol.21, No.1, pp. 433-434, 2006.

[6] R. J. Zhao, X. Lyu, Y. Fu, X. Hu, F. Li, "Coordinated Microgrid Frequency Regulation Based on DFIG Variable Coefficient Using Virtual Inertia and Primary Frequency Control", *IEEE Transactions on Energy Conversion*, Vol.31, No.3, pp.833-845, 2016.

[7] Y. Chen, J. Zhang, X. Chen, "Primary Frequency Regulation Control of Wind Turbines Based on Variable Power Tracking", In: *Proc. of IEEE International Conference on Advanced Information Technology, Electronic and Automation Control Conference (IAEAC)*, Chongqing, China, pp.2443-2449, 2018.

[8] Z. Lei, X. Sun, B. Xing, Y. Hu, and G. Jin, "Active Disturbance Rejection based MPPT Control for Wind Energy Conversion System under Uncertain Wind Velocity Changes", *Journal of Renewable And Sustainable Energy*, Vol.10, No.5, pp. 1-15, 2018.

[9] M. Chakib, T. Nasser, A. Essadki, "Comparative Study of Active Disturbance Rejection Control with RST

Control for Variable Wind Speed Turbine Based on Doubly Fed Induction Generator Connected to the Grid", *International Journal of Intelligent Engineering and Systems*, Vol.13, No.1, pp.248-258, 2020.

[10] J. Liu, H. Meng, Y. Hu, Z. Lin, W. Wang, "A Novel MPPT Method for Enhancing Energy Conversion Efficiency Taking Power Smoothing into Account", *Energy Conversion and Management*, Vol.101, pp.738-748, 2015.

[11] S. Ataee, H. Bevrani, "Improvement of Primary Frequency Control by Inertial Response Coordination Between Wind and Conventional Power Plants", *International Transactions on Electrical Energy Systems,* Vol.27, No.8, pp.1-12, 2017.

[12] K. V. Vidyanandan, N. Senroy, "Primary Frequency Regulation by Deloaded Wind Turbines using Variable Droop", *IEEE Trans. Power Systems*, Vol.28, No.2, pp. 837-846, 2013.

[13] E. Jahan, M. R. Hazari, S. M. Muyeen, A. Umemura, R. Takahashi, J. Tamura, "Primary Frequency Regulation Of The Hybrid Power System By Deloaded PMSG-Based Offshore Wind Farm using Centralized Droop Controller", *IET Journal of Engineering, The 7th International Conference on Renewable Power Generation (RPG)*, Vol.2019, No.18, pp. 4950-4954, 2018.

[14] M. Deepak, R. J. Abraham, F. M. Gonzalez-Longatt, D. M. Greenwood, H. S. Rajamani, "A novel approach to Frequency Support in a Wind Integrated Power System", *Renewable Energy An International Journal*, Vol.108, pp.194-206, 2017.

[15] C. Guo, D. Wang, "Frequency Regulation and Coordinated Control for Complex Wind Power Systems", *Hindawi Complexity*, Vol.2019, pp.1-12, 2019.

[16] M. C. Cheong, Z. Ma, H. Qian, J. Conger, P. Du, D. Chen, "Wind Turbine Participation in Primary Frequency Control", *Journal of Dynamic Systems, Measurement, and Control*, Vol.141, No.10, pp. 104501-1-6, 2019.

[17] X. Hua, X. Hongyuan, L. Na, "Control Strategy of DFIG Wind Turbine in Primary Frequency Regulation", In: *Proc. of IEEE International Conference on Industrial Electronics and Applications (ICIEA)*, Wuhan, China, pp.1751-1755, 2018.

[18] B. Motamed, P. Chen, M. Persson, "Comparison of Primary Frequency Support Methods for Wind Turbines", In: *Proc. of IEEE Grenoble Power Tech Conference*, Grenoble, France, pp.1-5, 2013.

[19] J. Dai, Y. Tang, Q. Wang, P. Jiang, "Aggregation Frequency Response Modeling for Wind Power Plants With Primary Frequency Regulation Service", *IEEE Accses*, Vol.7, pp.108561-108570, 2019.

[20] A. Nayak, M. K. Maharana, "Performance Assessment of Fuzzy Logic Controller for Load Frequency Control in Multi Source Multi Area System", *International Journal of Renewable Energy Research*, Vol.9, No.4, pp. 1597-1605, 2019.

[21] T. Banki, F. Faghihi, S. Soleymani, "Frequency Control of an Island Microgrid using Reset Control Method in the Presence of Renewable Sources and Parametric Uncertainty", *Systems Science & Control Engineering: An Open Access Journal*, Vol.8, No.1, pp. 500-507, 2020.

[22] R. Chakib, A. Essadki, M. Cherkaoui, "Modeling and Control of a Wind System based on a DFIG by Active Disturbance rejection control", *International Review on Modelling and Simulations (IREMOS)*, Vol.7, No.2, pp. 626-637, 2014

[23] J. Van de Vyver, T. Feremans, T. L. Vandoorn, J. D. M. De Kooning and L. Vandevelde, "Voltage based droop control in an islanded microgrid with wind turbines and battery storage", *International Conference on Renewable Energy Research and Applications (ICRERA)*, Palermo, pp. 612-617, 22-25 Nov 2015.

[24] A. Harrouz, I. Colak and K. Kayisli, "Control of a small wind turbine system application", *IEEE International Conference on Renewable Energy Research and Applications (ICRERA),* Birmingham, pp. 1128-1133, 20-23 Nov 2016.

[25] M. Doumi, I. Colak, A. G. Aissaoui, M. Abid, A. Tahour, " Robust MRAC for a wind turbine based on a doubly-fed induction generator", *IEEE International Conference on Renewable Energy Research and Applications (ICRERA),* San Diego, CA, pp. 1116-1165, 5-8 Nov 2017.

[26] M. R. Tur, M. Wadi, A. Shobole, S. Ay, "Load Frequency Control of Two Area Interconnected Power System Using Fuzzy Logic Control and PID Controller", *International Conference on Renewable Energy Research and Applications (ICRERA)*, Paris, pp. 1116-1165, 14-17 Oct. 2018.

[27] M. Ashglaf, C. Nichita, B. Dakyo, "Control Strategies Design for a Small-Scale Wind Turbine with a Doubly Fed Induction Generator", *IEEE International Conference on Renewable Energy Research and Applications (ICRERA)*, Paris, pp. 1092-1097, 14-17 Oct. 2018.